Title

Loss of cAMP Signaling in CD11c Immune Cells Protects Against Diet-Induced Obesity.

Journal

Diabetes, 72(9)

ISSN

0012-1797

Authors

Zeng, Liping

Herdman, D Scott

Lee, Sung Min

et al.

Publication Date

2023-09-01

DOI

10.2337/db22-1035

Peer reviewed

Loss of cAMP Signaling in CD11c Immune Cells Protects Against Diet-Induced Obesity

Liping Zeng,[1,2] D. Scott Herdman,[2] Sung Min Lee,[2] Ailin Tao,[1] Manasi Das,[2] Samuel Bertin,[2] Lars Eckmann,[2] Sushil K. Mahata,[2,3] Panyisha Wu,[2] Miki Hara,[4] Ji-Won Byun,[5] Shwetha Devulapalli,[6] Hemal H. Patel,[3,6] Anthony J.A. Molina,[2] Olivia Osborn,[2] Maripat Corr,[2] Eyal Raz,[2] and Nicholas J.G. Webster[2,3,7]

Diabetes 2023;72:1235–1250 | https://doi.org/10.2337/db22-1035

In obesity, CD11c$^+$ innate immune cells are recruited to adipose tissue and create an inflammatory state that causes both insulin and catecholamine resistance. We found that ablation of *Gnas,* the gene that encodes Gαs, in CD11c expressing cells protects mice from obesity, glucose intolerance, and insulin resistance. Transplantation studies showed that the lean phenotype was conferred by bone marrow–derived cells and did not require adaptive immunity. Loss of cAMP signaling was associated with increased adipose tissue norepinephrine and cAMP signaling, and prevention of catecholamine resistance. The adipose tissue had reduced expression of catecholamine transport and degradation enzymes, suggesting that the elevated norepinephrine resulted from decreased catabolism. Collectively, our results identified an important role for cAMP signaling in CD11c$^+$ innate immune cells in whole-body metabolism by controlling norepinephrine levels in white adipose tissue, modulating catecholamine-induced lipolysis and increasing thermogenesis, which, together, created a lean phenotype.

ARTICLE HIGHLIGHTS

- We undertook this study to understand how immune cells communicate with adipocytes, specifically, whether cAMP signaling in the immune cell and the adipocyte are connected.
- We identified a reciprocal interaction between CD11c$^+$ innate immune cells and adipocytes in which high cAMP signaling in the immune cell compartment induces low cAMP signaling in adipocytes and vice versa.
- This interaction regulates lipolysis in adipocytes and inflammation in immune cells, resulting in either a lean, obesity-resistant, and insulin-sensitive phenotype, or an obese, insulin-resistant phenotype.

Obesity is associated with a state of chronic, low-grade inflammation that contributes to insulin resistance and susceptibility to type 2 diabetes in rodents and humans (1). Recent studies have revealed that inflammation and metabolism are highly integrated. Diet-induced obesity (DIO) is characterized by the recruitment of immune cells, including CD11c$^+$ macrophages and dendritic cells (DCs), into adipose tissue (2). Tissue-resident immune cells in a lean animal generally have an anti-inflammatory phenotype, and DIO provokes trafficking of CD11c$^+$ monocyte-derived macrophages and DCs into adipose tissue (3). These recruited CD11c$^+$ immune cells are important factors in the pathogenesis of metabolic disease because their acute ablation attenuates adipose tissue inflammation and improves glucose tolerance (4).

[1]The Second Affiliated Hospital of Guangzhou Medical University, The State Key Laboratory of Respiratory Disease, Guangdong Provincial Key Laboratory of Allergy & Clinical Immunology, Guangzhou Medical University, China
[2]Department of Medicine, University of California San Diego, La Jolla, CA
[3]VA San Diego Healthcare System, San Diego, CA
[4]Center for Advanced Oral Science, Graduate School of Medical and Dental Sciences, Niigata University, Niigata, Japan
[5]Department of Dermatology, Inha University Hospital, Incheon, South Korea
[6]Department of Anesthesiology, University of California San Diego, La Jolla, CA
[7]Moores Cancer Center, University of California San Diego, La Jolla CA

Corresponding author: Nicholas J.G. Webster, nwebster@health.ucsd.edu

Received 19 December 2022 and accepted 21 May 2023

This article contains supplementary material online at https://doi.org/10.2337/figshare.23151608.

E.R. and N.J.G.W. are co-senior authors.

The G-protein Gαs (encoded by *Gnas*) regulates production of cAMP and mediates the sympathetic nervous system (SNS) effects on brown adipose tissue (BAT) to stimulate thermogenesis and promotes lipolysis on white adipose tissue (WAT) (5). Denervation of adipose tissue reduces both lipolysis and thermogenesis (6,7). Norepinephrine (NE) is the major effector of the SNS and stimulates adaptive thermogenesis and lipolysis through β-adrenergic receptors (β-ARs) (8). Mice lacking all β-ARs develop massive obesity due to a defect in stimulated lipolysis and a deficiency in diet-induced thermogenesis (9). Therefore, activation of BAT to increase energy expenditure via uncoupled thermogenesis is an attractive antiobesity strategy (10). Recently, brown adipocyte-like cells, also referred to as beige cells, have been described within WAT under thermogenic conditions and display similar physiological functions of brown adipocytes (11).

Here, we demonstrate that disruption of Gαs signaling in $CD11c^+$ innate immune cells improved glucose metabolism in mice by promoting energy expenditure and inducing adipose beiging, consequently preventing obesity and insulin resistance. Notably, we identified an important role for Gαs in $CD11c^+$ innate immune cells to regulate adipose tissue catecholamine levels that likely contribute to the lean phenotype that constitutes a potential target for the treatment of obesity.

RESEARCH DESIGN AND METHODS

Full, detailed methods are given in the online Supplementary Methods.

Mouse Studies

$Gnas^{\Delta CD11c}$ knockout [$Gnas^{tm5.1Lsw/tm5.1Lsw}$/*Tg(Itgax-cre)1–1Reiz*] mice (hereafter, KO mice) were generated from $Gnas^{fl/fl}$ ($Gnas^{tm5.1Lsw/tm5.1Lsw}$) mice (hereafter, Flox mice), as previously described (12). *Rag.ΔCD11c* mice were generated by crossing $Rag1^{-/-}$ mice with $Gnas^{\Delta CD11c}$ mice. Mice were housed inside a clean specific pathogen–free barrier facility. Under these conditions, mice up to 6 months of age are atopic with elevated IgE levels, but in the absence of an immunological challenge, their lungs and airways do not show any histological changes that would indicate an allergic response, lung CD4 and CD8 T-cell numbers are not altered, and cytokines are unchanged (12). Metabolic studies were performed in a Comprehensive Laboratory Animal Monitoring System. Glucose, insulin, and lipid tolerance tests were performed as published previously (13). For bone marrow transplantation, wild-type (WT) mice were lethally irradiated and then reconstituted intravenously with 6×10^6 bone marrow cells harvested from age- and sex-matched KO or Flox donor mice on the day after the irradiation. All the recipients received sulfamethoxazole and trimethoprim in drinking water for 2 weeks after irradiation. All procedures were approved by the Institutional Animal Care and Use Committee of the University of California San Diego, School of Medicine.

Flow Cytometry

Epididymal fat pads were digested with 1 mg/mL collagenase type II supplemented with 1% fetal BSA for 30 min at 37°C with shaking. Cell suspensions were filtered through a 100-μm filter and centrifuged at 2,000*g* for 10 min. The pellet containing the stromal vascular cells (SVCs) was then incubated with red blood cell lysis buffer and recentrifuged. The SVCs were resuspended in PBS with 2% FBS, incubated with fluorescently labeled primary antibodies for 30 min on ice and then analyzed on a Cytoflex flow cytometer.

Measurement of Catecholamines

NE, epinephrine (Epi), and dopamine (DA) were measured on a Waters ultra performance liquid chromatography (UPLC) system after alumina extraction, followed by separation and analysis with high-performance liquid chromatography. Dihydroxybenzylamine was used as an internal standard in each tissue sample. The data were analyzed with Empower software.

Protein and mRNA expression

Western blots and quantitative PCR assays were perfomed using standard procedures. Primers and antibodies are listed in supplementary tables. Hormones and cytokines were measured using commercial assays, as listed in supplementary tables.

Statistics

Data were analyzed using Prism software and are presented as mean ± SEM or mean ± SD. Statistical significance was determined using the unpaired two-tailed Student *t* test or one- or two-way ANOVA followed by Tukey post-tests for multiple variables. A P value of <0.05 was considered significant. Calorimetric data were analyzed by general linear regression models using body mass or activity as covariates using the CalR (14).

Data and Resource Availability

All data are available upon request from the corresponding author. The mice generated in this study are available from the University of California San Diego under a universal material transfer agreement.

RESULTS

Loss of cAMP Signaling in $CD11c^+$ Cells Confers Insulin Sensitivity and Resistance to Weight Gain

Mice with deletion of *Gnas* and cAMP signaling in $CD11c^+$ cells (KO) and control mice (Flox) have been described previously (12). In addition to the published immune phenotype, these mice have an unexpected metabolic phenotype. The body weight (BW) of both male and female KO mice on a normal chow diet (NCD) was significantly lower than that of control littermate Flox mice (Fig. 1*A*). At 5 months, male KO mice showed improved glucose tolerance (Fig. 1*B*). An insulin tolerance test (ITT) using a standard insulin

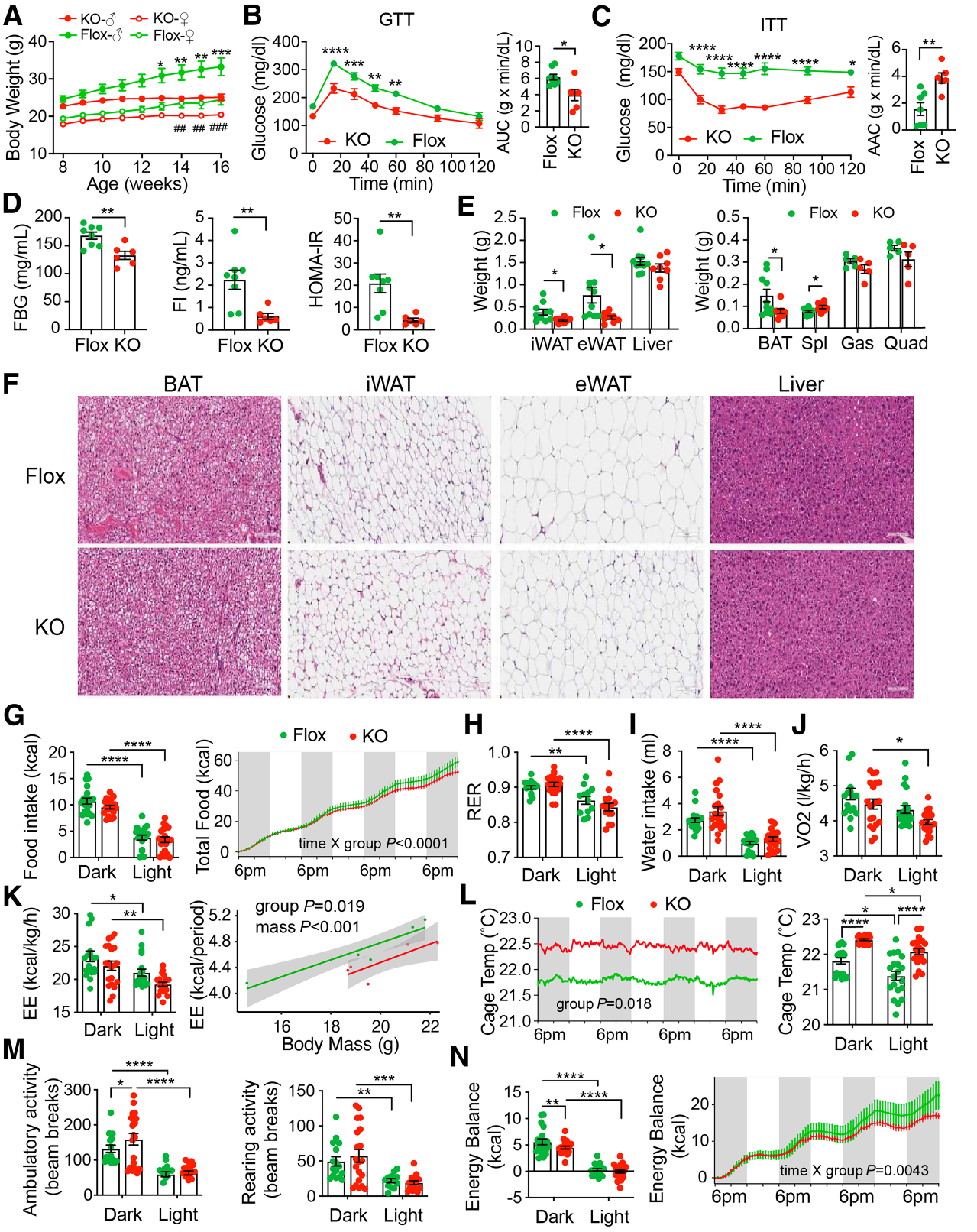

Figure 1—*Gnas*$^{\Delta CD11c}$ KO mice are glucose tolerant, insulin sensitive, and are protected from weight gain when fed normal chow. For all panels, Flox mice are shown in green, KO mice in red. *A*: BWs of male and female littermates fed an NCD from age 8 to 16 weeks (n = 8–10/group). Data are represented as mean ± SEM and asterisks (males) or hashtags (females) indicate statistical significance by two-way repeated measures ANOVA. *$P < 0.05$, **,##$P < 0.01$, ***,###$P < 0.001$. *B*: Glucose tolerance tests (2 g/kg D-glucose) of male mice fed an NCD. Two-way repeated measures ANOVA indicates significant genotype, time, and interaction effects (P = 0.0009, <0.0001, 0.0089, respectively). Bar graph shows area under the curve (AUC). *C*: ITTs (0.4 units/kg insulin) of male mice fed an NCD. Two-way repeated

dose (0.6 units/kg) caused severe hypoglycemia in the KO mice and the mice had to be rescued with a bolus of glucose (Supplementary Fig. 1*A*). Repeating the ITT with a lower dose of insulin (0.4 units/kg) showed that KO mice have improved insulin sensitivity (Fig. 1*C*), had lower fasting insulin and glucose levels, and, consequently, lower HOMA of insulin resistance (HOMA-IR) compared with control mice (Fig. 1*D*). Adipose tissue weights were lower in the KO mice. (Fig. 1*E*). Liver, BAT, epididymal WAT (eWAT), or inguinal WAT (iWAT) histologies were indistinguishable between genotypes (Fig. 1*F*), and adipocyte size distribution was the same (Supplementary Fig. 1*B*).

In metabolic cages, BW-matched KO mice consumed the same amount of food during dark and light phases but they ate a slightly lower cumulative amount of food (Fig. 1*G*). Respiratory exchange ratio (RER), water intake, V_{O_2}, and energy expenditure (EE) showed the expected circadian changes between dark and light phases, but there were no between genotypes (Fig. 1*H–K*, raw data shown in Supplementary Fig. 1*C–E*). Cumulative water consumption was increased in the KO, but EE was unchanged (Supplementary Fig. 1*F* and *G*). Covariate analysis of EE indicated significant body mass and genotype effects with lower EE for a given body mass in KO mice (Fig. 1*K*). Similar results were found for V_{O_2} and V_{CO_2} (Supplementary Fig. 1*H*). Despite lower EE, the cage temperatures were elevated in cages containing the KO mice during both the light and dark phases (Fig. 1*L*). Ambulatory locomotor activity was slightly elevated in the KO mice in the dark phase (Fig. 1*M*) and showed the expected circadian changes (Supplementary Fig. 1*I*). These results indicated that KO mice had a lean phenotype, which was associated with increased glucose and insulin tolerance, decreased food consumption, increased activity, and increased heat production in the face of reduced oxidative energy expenditure, culminating in decreased energy balance compared with Flox mice (Fig. 1*N*).

Loss of cAMP Signaling in CD11c$^+$ Cells Prevents High-Fat Diet–Induced Obesity

We then challenged the mice with a high-fat diet (HFD). Both male and female KO mice showed resistance to HFD-induced BW gain (Fig. 2*A*). Flox mice fed the HFD showed the expected whitening of the BAT (Fig. 2*B*), with adipocyte enlargement in eWAT (Fig. 2*C*) and iWAT (Supplementary Fig. 1*K*) and hepatic steatosis, but the KO mice did not have any of these changes. The KO mice had reduced adipose tissue by DEXA (Fig. 2*D* and Supplementary Fig. 1*L*), but bone density was unchanged (Supplementary Fig. 1*M*). Tissue weights of iWAT, eWAT, BAT, and liver were significantly lower in the KO mice after euthanasia (Fig. 2*E*). Consistent with their lean phenotype, KO mice had improved glucose tolerance in both males and females (Fig. 2*F*), as well as improved insulin sensitivity (Fig. 2*G*). A lipid tolerance test showed no alteration in lipid absorption (Fig. 2*H*). The temperature was elevated in metabolic cages containing KO mice, particularly during the light phase, as we observed before (Supplementary Fig. 1*N*). Cumulative food and water intakes were unchanged (Supplementary Fig. 1*O* and *P*). Diurnal changes in RER were suppressed in both genotypes due to the high fat content of the diet (Supplementary Fig. 1*Q*). V_{O_2}, EE, and V_{CO_2} values were similar between genotypes (Supplementary Fig. 1*R–T*), and covariate analysis did not indicate a significant body mass or genotype effect for mice on the HFD. Unlike mice fed the NCD, there was no difference in physical activity of energy balance in mice fed the HFD (Supplementary Fig. 1*U* and *V*).

Flow cytometric analysis of the SVCs from eWAT (Supplementary Fig. 2*A*) indicated reduced cellular content per gram of fat in the KO eWAT and reduced CD45$^+$ cells as a percentage of SVCs (Fig. 2*I*), reduced adipose tissue macrophages (ATMs) with decreased M1 and increased M2 (Fig. 2*J*), and decreased adipose tissue DCs (ATDCs) with decreased conventional type 1 DCs (cDC1) and increased conventional type 2 DCs (cDC2) (Fig. 2*K*) but increased eosinophils (Fig. 2*L*). Analysis of macrophage markers by quantitative (QPCR) indicated an increase in *Adgre1* (EMR1) and *Itgax* (CD11c) in eWAT from WT mice fed an HFD that was not seen in KO mice, but an increase in *Itgam* (CD11b) in KO mice consistent with the reduced M1 to M2 ratio (Fig. 2*M*). Comparing the overall populations, the KO mice had a reduced proportion of CD45$^+$ cells with decreased proportions of macrophages and DCs (Fig. 2*N*). A similar

measures ANOVA indicates significant genotype, time, and interaction effects ($P < 0.0001$, <0.0001, 0.009, respectively). Bar graph shows area above the curve (AAC). *D*: Fasting insulin and glucose levels and HOMA-IR of Flox and KO mice at 20 weeks. *E*: Tissue weights after sacrifice at 20 weeks. *F*: Histology of BAT, iWAT, eWAT, and liver by hematoxylin and eosin staining. *G*: Daily and cumulative food intake (kcal) during metabolic assessment. Gray shading indicates dark periods (lights off at 6 P.M.). Two-way ANOVA indicated a significant period effect ($P < 0.0001$). Repeated measures two-way ANOVA on cumulative intake indicated a significant time by group effect ($P < 0.0001$). *H*: RER during dark and light phases (significant period effect, $P < 0.0001$). *I*: Water intake during dark and light phases (significant period and genotype effects, $P < 0.0001$ and 0.024, respectively). *J*: V_{O_2} during dark and light phases (significant period and genotype effects, $P = 0.0003$ and 0.0132, respectively). *K*: Absolute EE during dark and light phases (significant period and genotype effects, $P < 0.0001$ and 0.0109, respectively), and body mass dependence during the light phase. Covariate analysis by general linear regression modeling indicated significant body mass and genotype effects ($P < 0.001$ and 0.019, respectively). EE during the dark phase did not show mass or genotype dependence. *L*: Cage temperature over course of assessment (genotype effect, $P = 0.018$) and average cage temperature for light and dark phases (significant period and genotype effects, $P < 0.0001$ for both). *M*: Ambulatory and rearing activity during dark and light phases (significant period effects, $P < 0.0001$ for both). *N*: Energy balance by dark and light phases (significant period effects, $P < 0.0001$) and cumulative energy balance. Repeated measures two-way ANOVA indicated a significant time by group effect ($P = 0.0043$). Data are represented as mean ± SEM and asterisks indicate statistical significance by two-way repeated measures ANOVA, two-way ANOVA, or unpaired Student *t* test as appropriate. *$P < 0.05$, **$P < 0.01$, ***$P < 0.001$, ****$P < 0.0001$ for genotype comparison or as indicated. ACC, area above the curve; Gas, gastrocnemius muscle; GTT, glucose tolerance test; Quad, quadriceps muscle; Spl, spleen.

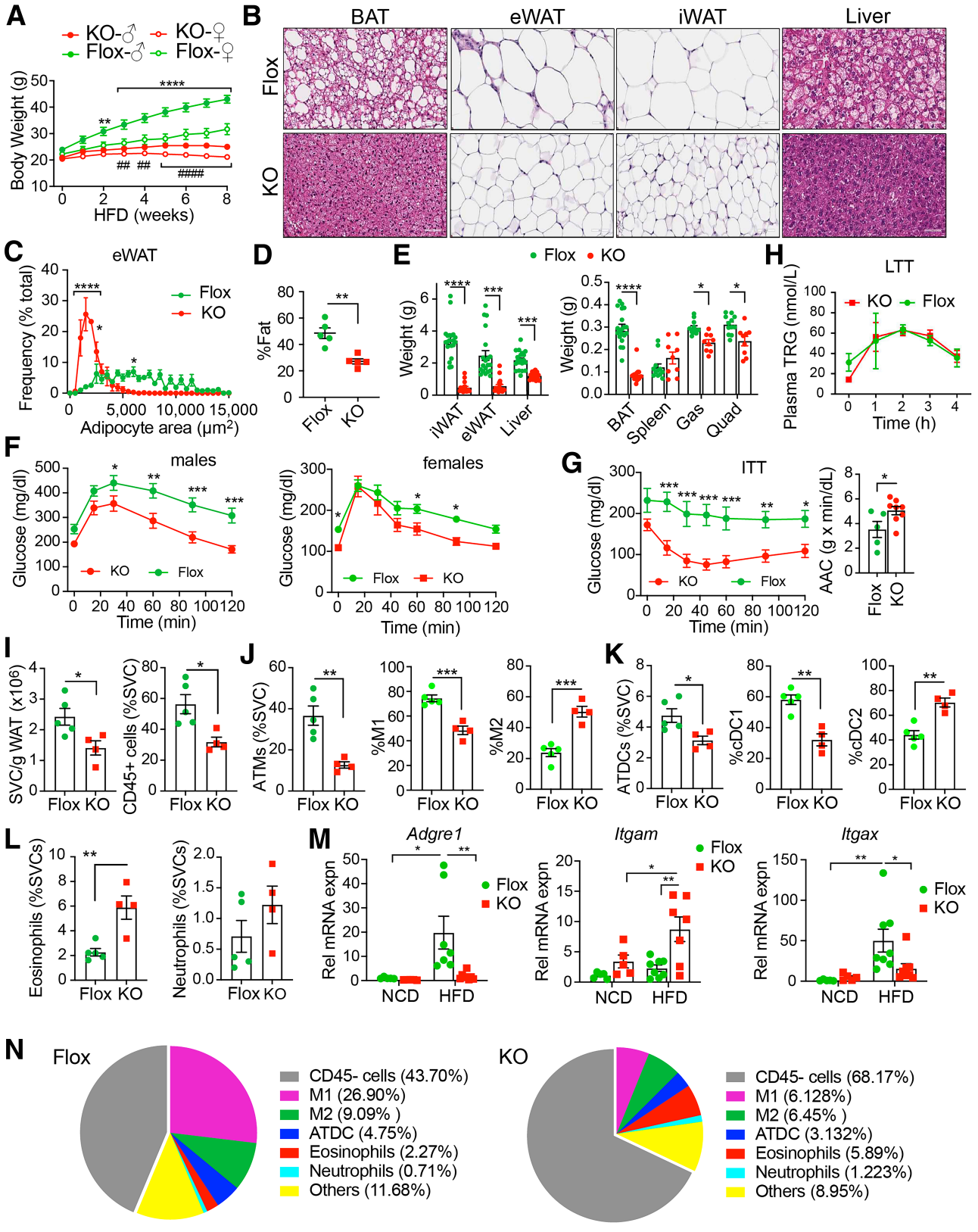

Figure 2—*Gnas*$^{\Delta CD11c}$ KO mice are protected from DIO when fed an HFD. *A*: BWs of male and female Flox and KO mice fed a 60% HFD were recorded for 8 weeks starting at 8 weeks of age (n = 19–20 for males and n = 8–12 for females). Flox mice are shown in green, KO mice in red. Asterisks indicate statistically significant genotype differences for male mice, hashtags indicate significant differences for female mice by repeated measures two-way ANOVA. *B*: Representative hematoxylin and eosin staining of BAT, eWAT, iWAT, and liver of HFD-fed Flox and KO mice. Scale bar = 100 μm. *C*: Adipocyte area distribution in eWAT from male Flox and KO mice fed an HFD. *D*: Adipose tissue by DEXA showing percentage of fat. *E*: Tissue weights of Flox and KO mice after 8 weeks of HFD feeding. iWAT, eWAT,

analysis of iWAT showed decreased numbers of ATMs, ATDCs, and eosinophils but increased numbers of neutrophils in the KO mice (Supplementary Fig. 2*B*) and the same M1→M2 and cDC1→cDC2 phenotype switch (Supplementary Fig. 2*C*). Unlike the eWAT, nonmyeloid immune cells composed the greatest proportion of cells in iWAT (Supplementary Fig. 2*D*), which likely represents B and T cells from the inguinal lymph node within the inguinal fat pad.

The difference in metabolic phenotype between NCD and HFD was not caused by the composition of the diet. Metabolic profiling during a diet-switch protocol showed that switching lean mice to the HFD alters circadian rhythms in oxidative metabolism, RER, and EE, and increased V_{O_2} and EE in both genotypes; however, differences in cage temperatures were still observed (Supplementary Fig. 3).

Hematopoietic Cells Are Responsible for the Lean Phenotype

CD11c is expressed on multiple hematopoietic cells but is also expressed on microglia in the brain (3). To assess the role of hematopoietic cells in the lean phenotype, we generated chimeric mice by transplanting bone marrow from KO or Flox donor mice (CD45.2) into lethally-irradiated, WT C57BL/6J recipient mice (CD45.1), which were then fed the HFD (Fig. 3*A*). Mice receiving KO donor cells started losing weight 3 weeks after bone marrow transplant (BMT) (Fig. 3*B*), despite greater weekly food intake (Fig. 3*C*). iWAT and eWAT were depleted when mice were sacrificed 8 weeks after BMT, but the liver and spleen were normal (Fig. 3*D*).

We assessed engraftment by measuring the percentage of donor CD45.2 cells in peripheral blood mononuclear cells (Supplementary Fig. 4*A*). Engraftment was 85–90% for both genotypes (Fig. 3*E*). We also assessed tissue engraftment of donor cells in eWAT (Supplementary Fig. 4*B*). Most (70–80%) of SVCs were derived from the donor mice (Fig. 3*F*). The mice had significantly more CD4 T cells and fewer ATMs when the bone marrow was transplanted from the KO mice (Fig. 3*G*). Engraftment into iWAT was similar (Supplementary Fig. 4*C*).

We then repeated the BMT but used recipient mice that had been made obese by 8 weeks of HFD feeding prior to the BMT to test whether the KO bone marrow could reverse the obese phenotype. Mice receiving the KO bone marrow started to lose weight 7 weeks after BMT (Fig. 3*K*) despite no change in food intake (Fig. 3*L*). The Flox and KO chimeric mice did not show a difference in glucose tolerance at 7 weeks (Fig. 3*M*), but the KO chimeric mice had improved insulin sensitivity and glucose tolerance at weeks 8 and 9 after BMT compared with the Flox chimeric mice (Fig. 3*L* and *M*), and this was still evident at week 11 (Supplementary Fig. 4*D*). These results suggested that lack of Gαs in bone marrow–derived immune cells is sufficient for metabolic improvement and resistance to DIO.

To determine whether T or B cells played a role in the metabolic improvement, we generated $Rag1^{-/-}/Gnas^{\Delta CD11c}$ double-KO mice ($Rag^{\Delta CD11c}$). The resulting $Rag^{\Delta CD11c}$ mice were resistant to DIO when fed an HFD (Fig. 3*N*) and consequently had reduced iWAT and eWAT (Fig. 3*O*). The $Rag^{\Delta CD11c}$ mice had decreased lipid accumulation in BAT and smaller adipocytes in eWAT and iWAT (Supplementary Fig. 5*A*). The mice also had improved glucose tolerance and insulin sensitivity (Fig. 3*P* and *Q*) and decreased fasting blood glucose levels (Fig. 3*R*), insulin levels (Fig. 3*S*), and HOMA-IR (Fig. 3*T*) relative to $Rag^{fl/fl}$ controls. Metabolic studies of the $Rag^{\Delta CD11c}$ mice fed an HFD showed reduced food intake, EE, and V_{O_2} and V_{CO_2}, relative to the $Rag^{fl/fl}$ control mice (Supplementary Fig. 5*B–D*). Interestingly covariate analysis of the data against locomotor activity, but not body mass, showed that the $Rag^{\Delta CD11c}$ mice expended less energy and consumed fewer calories for the equivalent activity (Supplementary Fig. 5*E*). These results suggested that adaptive immunity was not required for the lean phenotype. Deletion of *Gnas* in macrophages using LysM-Cre did not confer a lean phenotype (Supplementary Fig. 6*A–C*) nor did altering the gut microbiota by cohousing or fecal transfer (Supplementary Fig. 6*D–F*).

Defective Cold Response but Increased Thermogenesis in $Gnas^{\Delta CD11c}$ KO Mice

As the cage temperature was increased in metabolic cages containing KO mice, we investigated body temperature of Flox and KO mice by using infrared imaging. We observed increased temperature in the KO mice as compared with Flox mice, especially those fed an HFD (Fig. 4*A*). Because KO mice have reduced adipose tissue, we tested whether the KO mice could adapt to a cold challenge. The Flox mice

BAT, liver, gastrocnemius muscle (Gas), and quadriceps muscle (Quad). *F*: Glucose tolerance test (GTT) results for mice fed an HFD and AUC. Significant time ($P < 0.0001$), genotype ($P = 0.0029$), and interaction ($P = 0.055$) by repeated measures two-way ANOVA. *G*: ITT for mice fed an HFD and area above the curve (AAC). Significant time ($P < 0.0001$), genotype ($P = 0.005$), and interaction ($P < 0.0001$) by repeated measures two-way ANOVA. *H*: Lipid tolerance test (LTT) results of mice given a bolus of sesame oil. Graph indicates plasma triglyceride (TRG) levels. *I*: Flow cytometry analysis of SVCs from eWAT. Total number of SVCs per gram of tissue and percentage of $CD45^+$ cells in SVC. *J*: ATMs as a percentage of SVC. Proportion of M1 and M2 macrophages as a percentage of ATM. *K*: ATDCs. Proportion of $CD11b^+$ cDC1 and $CD11b^+$ cDC2 subsets of DCs as %ATDC. *L*: Eosinophils and neutrophils as percentages of SVC. *M*: Expression of *Adgre1* (Emr1), *Itgax* (CD11c), and *Itgam* (CD11b) by QPCR from eWAT RNA. *N*: Pie chart showing relative proportions of cells in iWAT from Flox and KO mice. Data are presented as percentage of SVCs. Data are represented as mean ± SEM and asterisks indicate statistical significance by two-way repeated measures ANOVA or unpaired Student *t* test as appropriate. $*P < 0.05$, $**P < 0.01$, $***P < 0.001$, $****P < 0.0001$ for genotype comparison or as indicated.

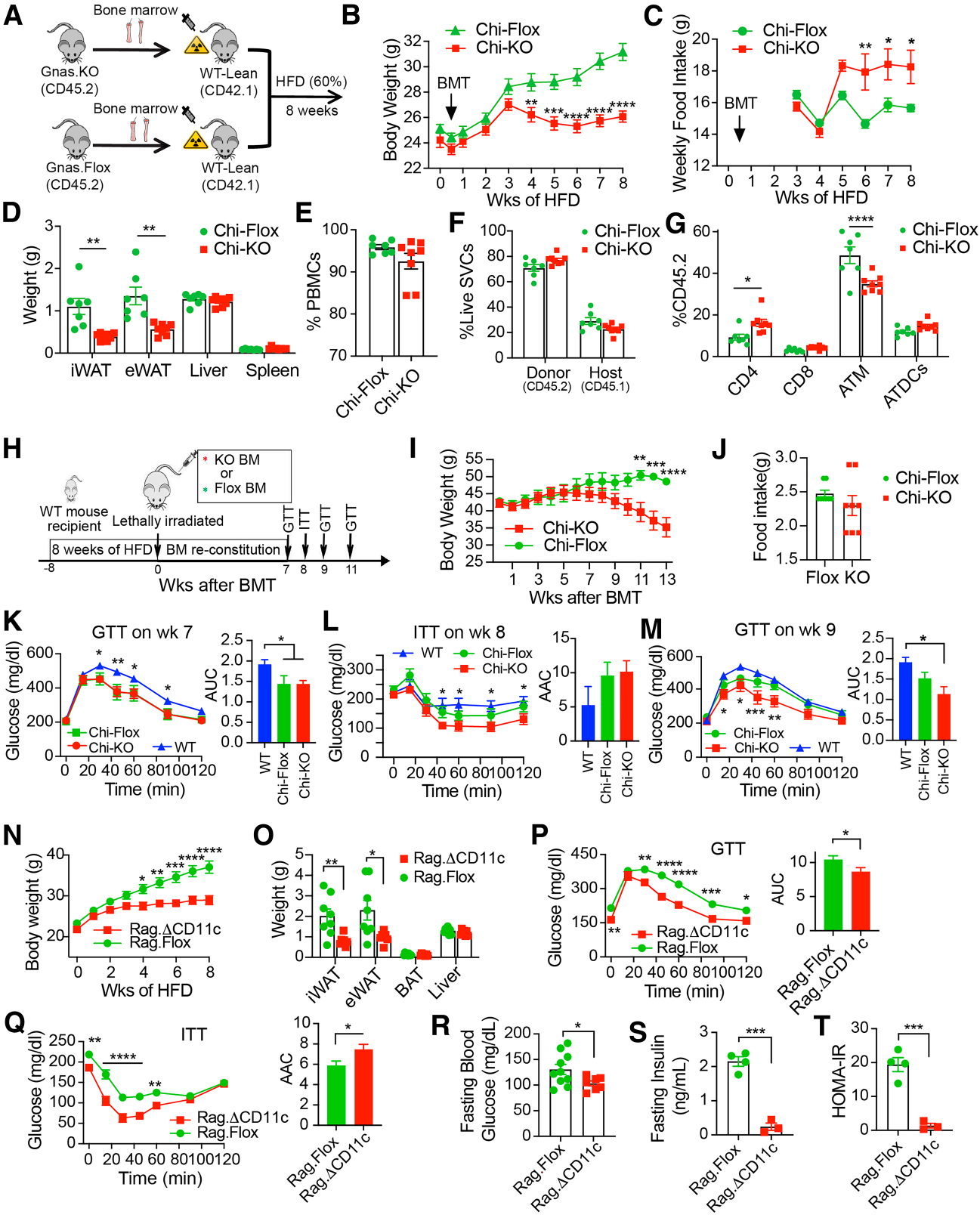

Figure 3—Hematopoietic cells are responsible for the lean phenotype of *Gnas*$^{\Delta CD11c}$ KO mice. *A*: Schematic of BMT into lean recipient mice that are then fed an HFD for 8 weeks. *B*: BW of chimeric mice after BMT with bone marrow from KO mice (chi-KO; red) or Flox mice (chi-Flox; green). Repeated measures two-way ANOVA indicated significant time and genotype × time interaction ($P < 0.0001$ and <0.0001). *C*: Weekly food intake for chi-KO and chi-Flox recipients starting 3 weeks after BMT. *D*: Tissue weights at sacrifice. *E*: Percentage of engraftment of donor bone marrow cells (CD45.2) in peripheral blood mononuclear cells. *F*: Percentage of donor cells (CD45.2) from Flox or KO mice and host cells (CD45.1) in SVCs from eWAT. *G*: Percentage of donor cells in CD4 and CD8 T cells, ATM, and ATDC

were able to maintain their body temperature, but the body temperature of KO mice dropped by almost 5°C after 4.5 h (Fig. 4*B*). Body temperature quickly recovered when mice were removed from the cold room. This suggested either a defective adrenergic response to cold or defective thermogenesis. To assess the thermogenic capacity of various tissues, we performed an oxygen flux analysis using an Oroboros system. Isolated soleus muscle, an oxidative slow-twitch muscle, showed increased basal oxidative phosphorylation, increased maximal mitochondrial complex I activity, increased complex I+II activity, and increased maximal uncoupled activity (Fig. 4*C*). The glycolytic fast-twitch gastrocnemius muscle did not show these alterations (Supplementary Fig. 7*A*) nor did BAT or liver (Supplementary Fig. 7*B* and *C*), although liver showed greater uncoupled complex II activity. Oxygen flux measurements in eWAT and iWAT, however, were indistinguishable from baseline noise. To determine if the immune cells could contribute to the change in oxidative metabolism, we analyzed splenic $CD11c^+$ cells on a Seahorse instrument. Cells from KO mice had elevated basal respiration that was primarily driven by an increase in ATP-linked respiration (Fig. 4*D*) rather than an increase in proton leak.

To assess the thermogenic potential of WAT, we measured UCP1 expression by Western blot. UCP1 protein was increased in eWAT and iWAT but was reduced in BAT (Fig. 4*E*), so we then measured the expression of brown- and beige-associated genes. *Ucp1* mRNA was reduced in BAT, consistent with the protein data (Fig. 4*F*), as was expression of *Oplah*, *Pdk4*, and *Serca2b*, but it was highly elevated in eWAT, as was *Pgc1a*, *Cidea*, and *Pparg* expression (Fig. 4*G*). Changes in iWAT were less pronounced (Fig. 4*H*). Expression of adipose triglyceride lipase (ATGL/PNPLA2), the major lipase involved in basal lipolysis (15), and phosphorylation of hormone sensitive lipase (HSL/LIPE) on Ser563, the major lipase involved in cAMP-stimulated lipolysis, were increased in both iWAT and eWAT from mice fed an HFD (Fig. 4*I*). Phosphorylation of cAMP-dependent protein kinase (PKA) substrates was also increased in KO iWAT and eWAT (Supplementary Fig. 8*A*). In contrast, however, phosphorylation of p70S6Kinase on Thr389, which is repressed by PKA, was reduced in the KO WAT (Fig. 4*I*). We did not see phosphorylation of HSL or induction of UCP1 or ATGL in mice of either genotype that were fed the NCD (Supplementary Fig. 8*B*). These results indicate that cAMP signaling is selectively increased in WAT of KO mice fed the HFD.

Loss of *Gnas* in $CD11c^+$ Cells Paradoxically Increases cAMP Signaling in WAT

To test for a circulating factor that could increase cellular cAMP in adipocytes, we treated 3T3-L1 adipocytes with serum from either KO or Flox mice and found that both could increase intracellular cAMP levels (Fig. 5*A*). Treatment of 3T3-L1 adipocytes with serum from either Flox or KO mice fed an NCD activated HSL(Ser563), perilipin(Ser522), and CREB(Ser133) phosphorylation (Fig. 5*B*). Similar results were observed with serum from HFD-fed mice (Fig. 5*C*). The increase of cAMP and PKA signaling was blunted when the cells were pretreated with propranolol, suggesting activation of β-ARs. We then tested whether the presence of immune cells could influence the lipolysis response of 3T3-L1 adipocytes to the selective β3-adrenergic receptor agonist CL-316,243 (CL). CD11c bone marrow–derived macrophages (BMDMs) from the KO stimulated greater glycerol release from 3T3-L1 adipocytes in response to CL (1 μmol/L for 3 h) when cocultured in a Transwell or in contact culture compared with cells from Flox mice (Fig. 5*D*). Similar results were obtained with splenocytes from KO mice (Supplementary Fig. 9*A*). The communication in the coculture experiments was bidirectional as 3T3-L1 adipocytes altered cytokine expression in BMDM in the immune cells. BMDM from Flox mice had elevated levels of *Il1b* and *Il6* cytokine expression, which was further stimulated by the 3T3-L1 adipocytes, whereas BMDMs from KO mice had much lower cytokine expression and were refractory to 3T3-L1 stimulation (Fig. 5*E*).

NE and DA Are Elevated in WAT of *Gnas*$^{\Delta CD11c}$ KO Mice

The inhibition of serum-stimulated cAMP signaling by propranolol suggested β-adrenergic signaling, so we measured NE, Epi, and DA levels in plasma from Flox and KO mice. Plasma levels of NE and DA were not altered between KO and

in SVC from eWAT by flow cytometry. *H*: Schematic of BMT in obese recipient mice fed an HFD. *I*: BW of chimeric mice after BMT. Significant time and genotype × time interaction ($P < 0.0001$ and <0.0001). *J*: Daily food intake for chi-KO and chi-Flox recipients. *K*: Glucose tolerance tests (GTTs) performed 7 weeks after BMT for chi-KO and chi-Flox mice compared with control obese WT mice ($n = 8$/group). Significant time and genotype effects, and interaction ($P < 0.0001$, 0.0113, 0.0492, respectively). AUC is shown on right. *L*: ITTs for chi-KO and chi-Flox mice compared with obese WT mice ($n = 8$/group). Significant time and genotype × time interaction ($P < 0.0001$ and 0.036, respectively). Area above the curve (AAC) is shown on right. *M*: GTT performed 9 weeks after BMT ($n = 8$/group). Significant time and genotype effects, and interaction ($P < 0.0001$, 0.037, 0.0032, respectively). AUC is shown on right. *N*: BWs of *Rag1:Gnas*$^{\Delta CD11c}$ (Rag.ΔCD11c) and *Rag1:Gnas*$^{fl/fl}$ (Rag.Flox) mice fed a 60% HFD ($n = 11$–15/group). Significant time and genotype effects, and interaction ($P < 0.0001$, 0.0038, <0.0001, respectively). AUC is shown on right. *O*: Tissue weights for iWAT, eWAT, BAT, and liver of Rag.ΔCD11c and Rag.Flox mice after 8 weeks of HFD feeding ($n = 5$–8/group). *P*: GTT results for Rag.ΔCD11c and Rag.Flox mice after 8 weeks of HFD ($n = 6$–15/group). Significant time and genotype effects, and interaction ($P < 0.0001$, 0.0001, 0.0014 respectively). AUC is shown in the right-hand panels. *Q*: ITT results for Rag.ΔCD11c and Rag.Flox mice after 8 weeks of HFD ($n = 6$–15/group). Significant time and genotype effects, and interaction ($P < 0.0001$, <0.0001, 0.0002, respectively). AAC is shown in the right-hand panels. Fasting glucose (*R*), fasting insulin (*S*), and HOMA-IR (*T*) findings from HFD-fed Rag.Flox and Rag.ΔCD11c mice. For all graphs, data are presented as mean ± SEM and asterisks indicate statistical significance by unpaired Student *t* test or repeated measures two-way ANOVA as appropriate. *$P < 0.05$, **$P < 0.01$, ***$P < 0.001$, and ****$P < 0.0001$.

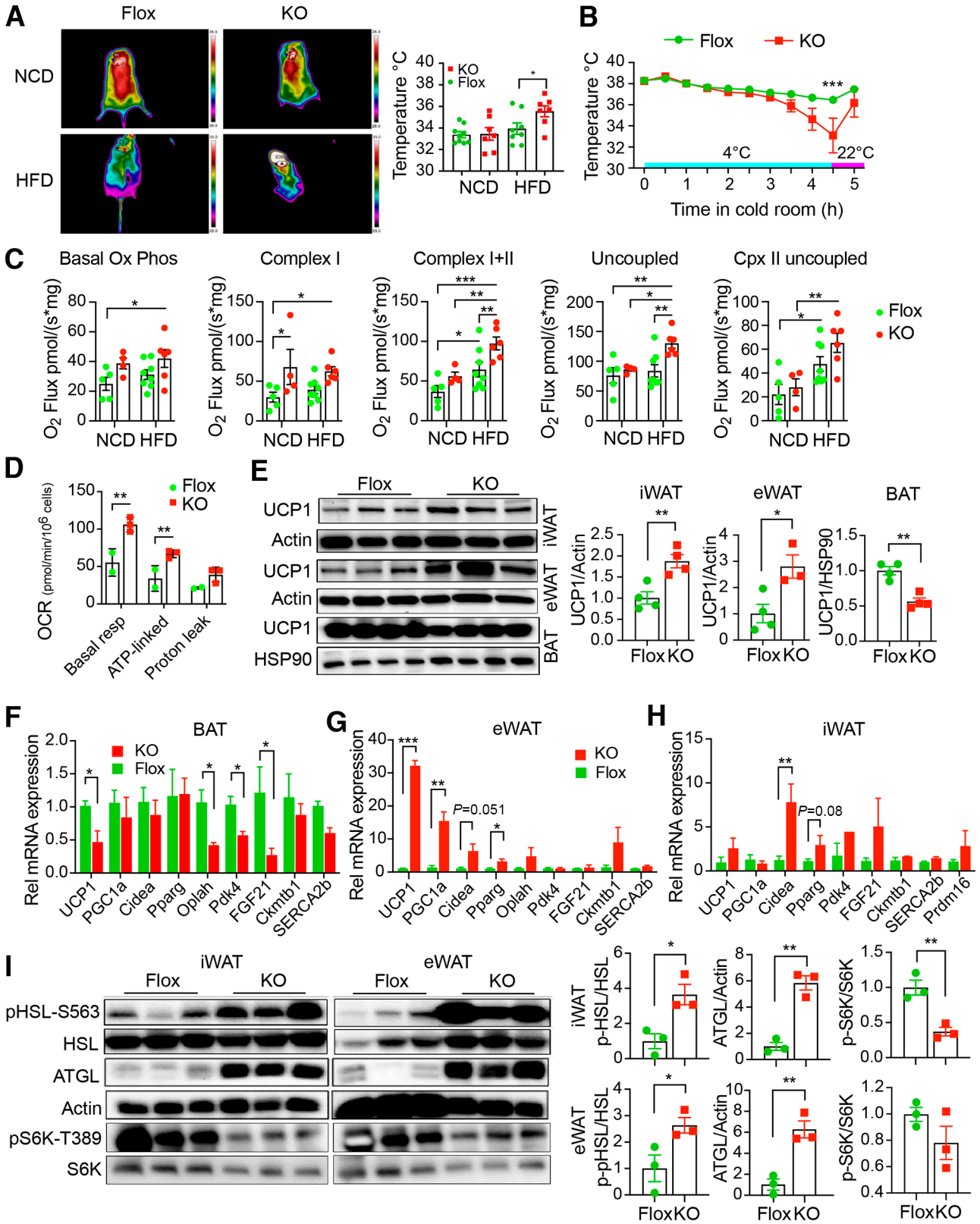

Figure 4—Impaired response to cold challenge, yet increased UCP1 expression in *Gnas*$^{\Delta CD11c}$ KO mice. *A*: Infrared thermography was used to quantify heat generation from the interscapular brown fat depot. Thermal camera images of dorsal view of Flox and KO mice fed with indicated diet (NCD or HFD). Quantification of BAT temperatures of mice from representative images (n = 7–9 mice/group). Flox mice are in green, KO mice in red. *B*: Cold-room challenge. Body temperatures of NCD-fed Flox and KO mice with subcutaneous temperature sensors placed in cold room at 4°C (n = 5/group). Cyan bar indicates period of 4°C, magenta indicates return to 22°C. Repeated measures two-way ANOVA indicated significant time and genotype × time interaction (P = 0.0039 and 0.0015, respectively). *C*: Oroboros oxygen

Flox mice (Fig. 5*G*), nor was plasma Epi level (Supplementary Fig. 9*B*). In contrast, tissue NE and DA levels were significantly higher in eWAT of KO mice under both NCD and HFD feeding (Fig. 5*H*). Similar NE increases were found in iWAT (Supplementary Fig. 9*C*), but DA was not detected in the majority of iWAT samples. Epi was not detected in either eWAT or iWAT, consistent with the sympathetic origin of the NE. Adrenal catecholamine levels did not change between genotypes or diets (Supplementary Fig. 9*D*).

To test WAT sensitivity to adrenergic stimulation, we challenged mice fed either the NCD or HFD with CL-316,243 and measured glycerol levels as a surrogate for lipolysis. Because the KO mice have much less WAT (Fig. 2*D*), we normalized the glycerol levels to the adipose tissue weight. Basal glycerol levels were increased in KO mice compared with Flox mice fed the NCD and were not suppressed by the HFD (Fig. 5*I*). Stimulated glycerol release was not different between genotypes but was reduced by the HFD. Raw glycerol levels were lower in the KO mice, reflecting the depleted adipose tissue lipids (Supplementary Fig. 9*E*). These results would indicate that a given amount of adipose tissue in KO mice is more lipolytic than the equivalent in Flox mice, and that the major genotype difference is seen in basal glycerol levels, consistent with the elevated ATGL (Fig. 4*I*). Because the stimulated glycerol levels were lower in mice fed the HFD, we measured β-AR expression. The adipocyte-specific β-3AR (*Adrb3*) was decreased dramatically in both eWAT and iWAT of Flox mice fed the HFD (Fig. 5*J*). *Adrb3* was partially reduced in the KO mice fed the NCD but did not change upon HFD feeding in either depot (Fig. 5*J*). In contrast, there were no changes in the expression levels of β-1AR (*Adrb1*) and β-2AR (*Adrb2*) between the groups or diets (Supplementary Fig. 9*F*).

To explore the cause of elevated catecholamine levels in the KO WAT, we measured expression of catecholamine transporters and enzymes of catecholamine synthesis and degradation. Expression of the organic cation transporter 3 (*Slc22a3*; OCT3) was decreased in the eWAT of KO mice fed the NCD, and the NE transporter (*Slc6a2*; NET) was decreased in the eWAT of KO mice fed the HFD (Fig. 5*K*). Expression of *Slc22a3* did not change significantly in iWAT (Supplementary Fig. 9*G*); however, *Slc6a2* was not detected. The expression of monoamine oxidase A (*Maoa*) was significantly increased in both eWAT and iWAT from Flox mice fed an HFD, and this increase was blunted in the KO mice. Expression of catecholamine-*O*-methyl transferase (*Comt*) was significantly lower in eWAT from KO mice but did not change in iWAT (Fig. 5*L* and Supplementary Fig. 9*H*). Expression of tyrosine hydroxylase (*Th*), the rate-limiting enzyme for catecholamine synthesis, was not detected in the WAT of Flox and KO mice and did not differ in the adrenal glands of KO and Flox mice (Supplementary Fig. 9*I*). Collectively, these data suggest that Gαs deficiency in $CD11c^+$ innate immune cells elevated tissue NE but prevented *Adrb3* downregulation, allowing continued adrenergic stimulation of the adipose tissue.

Gnas$^{\Delta CD11c}$ KO Mice Have Reduced Adipose Tissue Inflammation and cAMP Signaling Promotes the Inflammatory Phenotype of Immune Cells

Obesity is associated with immune cell infiltration and inflammation of adipose tissue. We observed fewer macrophage crown-like structures in the eWAT of KO mice compared with Flox mice fed the HFD, consistent with reduced inflammation (Fig. 6*A*). This was not due to a migratory defect, because BMDM migration in vitro was slightly increased in KO mice in response to 3T3-L1 adipocyte conditioned medium, but the response to serum was unchanged (Fig. 6*B* and Supplementary Fig. 10*A*). Migration of fluorescently labeled (PKH26) $CD11c^+$ BMDM into adipose tissue in vivo by flow cytometry (Supplementary Fig. 10*B*) showed that BMDMs from KO mice migrated to WAT in obese WT recipient mice to the same extent as cells from Flox mice (Fig. 6*C*). We then assessed chemokine and cytokine expression. In Flox mice, the HFD increased the expression of *Ccl2* and *Il6* that was markedly blunted in the KO mice (Fig. 6*D*). Plasma CCL2 was unchanged, however, and IL-6 was slightly elevated in KO mice fed the HFD (Fig. 6*E*). In contrast, *Il10* was increased in KO mice in either NCD or HFD groups, and IL-10 level was significantly higher (200 pg/mL; ∼50-fold) in the KO mice, especially those fed the HFD (Fig. 6*E*). No significant differences in the mRNA and circulating levels of TNFα or IL-1β were observed between the groups (Supplementary Fig. 10*C*).

Cytokine induction is mediated partly by increased expression and activation of the inflammasome, especially NLRP3. HFD induced NLRP3 protein expression and processing of pro-IL1β in eWAT in Flox mice, but this was absent in the KO mice (Fig. 6*F* and Supplementary Fig. 11*A*). Similarly, the inflammasome components *Caspase-1* and adaptor protein apoptosis-associated speck-like protein

flux analysis of isolated soleus muscle from flow or KO mice fed an NCD or HFD. Graphs show basal oxidative phosphorylation (Ox Phos), maximal complex (Cpx) I activity, maximal complex I+II activity, maximal uncoupled respiration (resp), and uncoupled complex II activity. Two-way ANOVA indicated significant genotype effects for OxPhos, Cpx I, CpxI+II, maximum uncoupled respiration ($P = 0.017$, 0.0041, 0.0089, 0.015, respectively), and a significant diet effect for Cpx II ($P = 0.0006$). *D*: Seahorse analysis of $CD11c^+$ cells isolated from spleen showing oxygen consumption rate (OCR) due to basal respiration, ATP-linked respiration, and proton leak (uncoupled respiration). Two-way ANOVA indicated significant genotype and group effects ($P = 0.0002$ and 0.0002) *E*: Representative immunoblots of UCP1 in iWAT, eWAT, and BAT of HFD-fed Flox and KO mice. Actin and HSP90 were used as loading controls. Graphs show quantification. *F–H*: Relative (Rel) expression of beige-related genes in BAT (*F*), eWAT (*G*), and iWAT (*H*) of HFD-fed Flox and KO mice normalized to m36B4 control mRNA ($n = 3$–4/group). *I*: Immunoblots for phospho-Ser563 HSL, total HSL, ATGL, phospho-Thr389 p70S6K, total S6K, and tubulin in iWAT and eWAT extracts from HFD-fed Flox and KO mice. Graphs show quantification ($n = 3$–4/group). Data are presented as mean ± SEM and asterisks indicate statistical significance by one- or two-way ANOVA or unpaired Student *t* test, as appropriate. $*P < 0.05$, $**P < 0.01$, $***P < 0.001$.

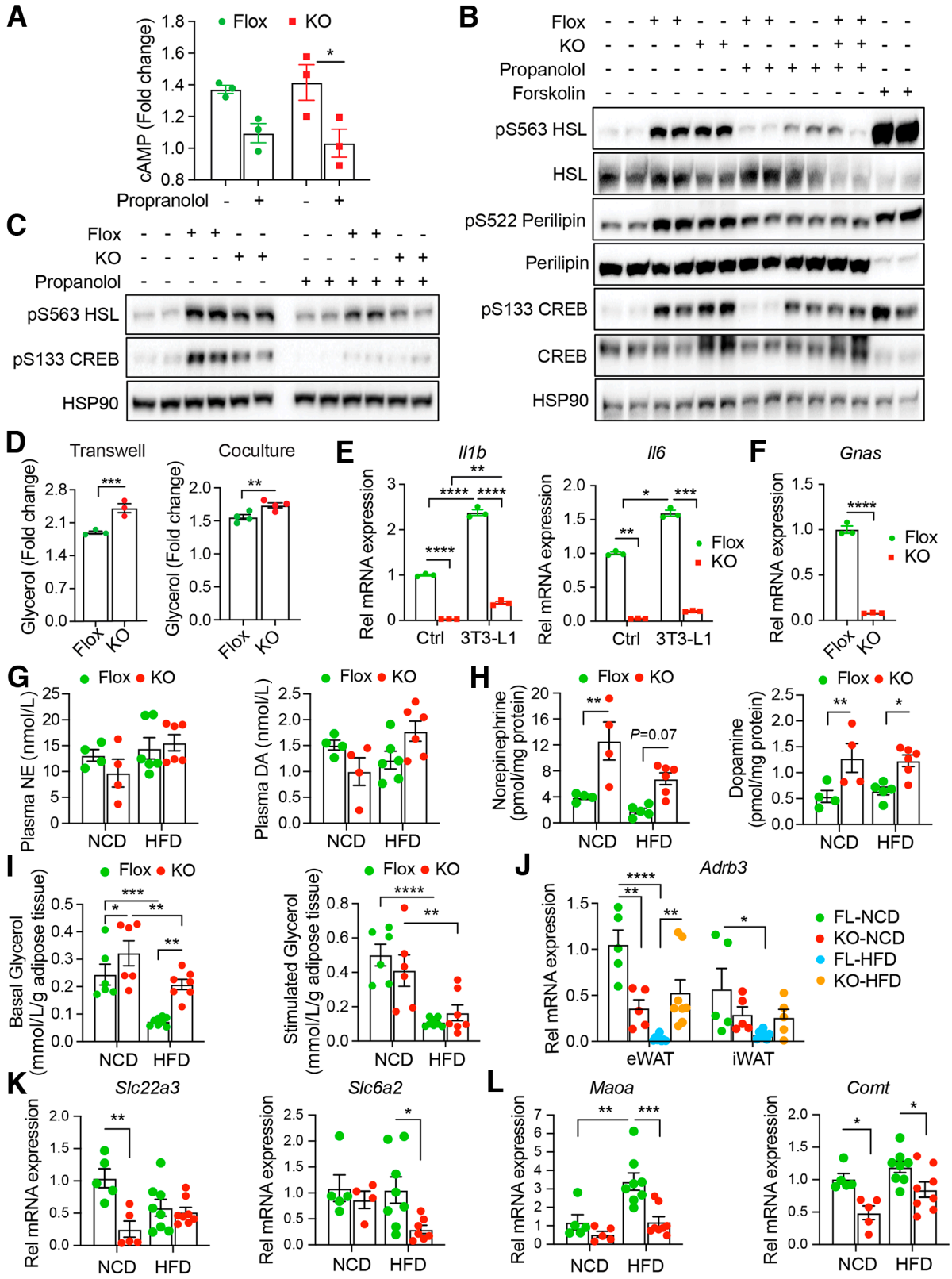

Figure 5—NE and DA levels are elevated and activate PKA signaling in WAT of *Gnas*$^{\Delta CD11c}$ KO mice. *A*: cAMP level in 3T3-L1 adipocytes treated with 3% serum from Flox or KO mice, with or without the nonselective β-AR blocker propranolol (50 μmol/L), by ELISA (*n* = 3/group). *B*: Immunoblot for the phosphorylation of HSL(Ser563), perilipin(Ser522), and CREB(Ser133) in 3T3-L1 adipocytes cells treated for 30 min with 3% serum from NCD-fed KO and Flox mice. HSP90 was used as loading control. *C*: Immunoblot for the phosphorylation of HSL(Ser563) and CREB(Ser133) in 3T3-L1 adipocytes cells treated for 30 min with 3% serum from HFD-fed KO and Flox mice. HSP90 was used as loading control. *D*: Fold change in glycerol levels in conditioned medium from 3T3-L1 adipocytes either with or without

containing a caspase-recruitment domain (*Pycard*) were induced by the HFD in Flox mice but not KO mice (Fig. 6*G*). Activation of the NLRP3 inflammasome by cAMP and lipopolysaccharide (LPS) was then tested in BMDMs as an in vitro model system. The induction of *Nlrp3*, *Il1b*, and *Il6* mRNAs by LPS was suppressed in the BMDMs from KO mice (Fig. 6*H*). We also detected decreased protein expression and secretion in the supernatants of KO BMDMs (Fig. 6*I* and *J*). As expected, *Gnas* expression was greatly reduced in KO BMDMs, but *TLR*, *MyD88*, and *Irf1–4* expression was unchanged, and *Trif*, *Irf7*, and *Klf4* expression was slightly elevated (Supplementary Fig. 11*B–D*). LPS induction of p38MAPK, JNK, and ERK was preserved (Supplementary Fig. 11*E*), but degradation of Iκb and phosphorylation of p65 RelA was impaired in KO BMDMs (Supplementary Fig. 11*F*), consistent with suppressed inflammatory signaling. Mechanistically, expression of PPARγ, a known repressor of NLRP3 (16,17), was much higher in KO BMDMs and decreased with LPS (Fig. 6*I*).

Taking a pharmacological approach, BMDMs from Flox and KO mice were treated with the cell-permeable cAMP analog 8-(4-chlorophenylthio) adenosine 3′,5′-cyclic monophosphate (CPT) or formoterol, a long-acting β2 agonist (LABA). CPT induced NLRP3 and pro-IL1β expression in both Flox and KO BMDMs, but LABA only worked in Flox BMDMs due to the lack of Gαs in the KO BMDMs (Fig. 6*K*). PPARγ expression was suppressed by CPT in BMDMs from both genotypes, but LABA, again, had no effect in KO BMDMs (Fig. 6*K*). At the mRNA level, CPT induced *Crem*, *Il1b*, and *Nlrp3* and repressed *Pparg* in BMDMs from both genotypes, but LABA had no effect in the KO BMDMs (Fig. 6*L* and *M*). Similar effects were observed with dibutyryl-cAMP, isoproterenol, and forskolin (Supplementary Fig. 11*G*). These data indicate that inflammatory signaling requires cAMP signaling in addition to TLR activation.

DISCUSSION

We report in this article the reciprocal regulation of cAMP signaling in $CD11c^+$ innate immune cells and adipocytes. Suppression of cAMP generation in $CD11c^+$ cells caused an anti-inflammatory phenotype in adipose tissue with, paradoxically, increased cAMP signaling in adipocytes, increased adipose tissue NE, and increased lipolysis and beiging. The increased NE was accompanied by decreased expression of catecholamine transporters and metabolizing enzymes, which we interpret to indicate that reduced tissue catecholamine clearance in immune cells was the primary cause of the elevated NE. The cumulative effects of these changes were to create a lean, obesity-resistant phenotype (Fig. 7). The effect was mediated by bone marrow–derived cells and did not require adaptive immunity. Although our results support the importance of cAMP signaling in both the innate immune cell and adipocyte compartments and the interaction between these cell types to coordinate sympathetic regulation of adipose tissue function, we cannot exclude effects outside of the adipose tissue, because CD11c immune cells are found in many other tissues. Indeed, we see increased oxidative metabolism in selected slow-twitch muscles that may contribute to the phenotype.

That selective elevation of Gαs signaling and lipolysis in adipocytes could explain the observed phenotype is supported by evidence that selective chemogenetic activation of Gαs in adipocytes increases energy expenditure, improves glucose metabolism, and decreases fat mass (18), and deletion of Gαi2 in adipocytes similarly protects against DIO (19). Conversely, genetic deletion of Gαs in adipocytes reduces lipolysis and impairs thermogenesis (20). If Gαs is deleted in both adipocytes and immune cells, the phenotype is very different because the KO mice are lean, have severely reduced adipose tissue, impaired glucose tolerance, and reduced thermogenic response to catecholamines or diet (21), suggesting that the loss of Gαs in immune cells is dominant over the effect of Gαs loss in adipocytes.

The connection between sympathetic activity and adipose tissue lipolysis has been studied in both animal models and humans (22–25). Peripheral sympatho-facilitators or direct optogenetic stimulation of adipose tissue sympathetic nerves activate lipolysis and cause fat mass loss

CL-316,243 (1 μmol/L) stimulation after culture with BMDMs derived from Flox or KO mice in Transwell inserts or in contact coculture. *E*: Cytokine gene expression in BMDMs after culture in Transwell inserts in the presence of 3T3-L1 adipocytes by QPCR. *F*: Expression of *Gnas* gene in BMDMs. *G*: Plasma NE and DA levels from NCD-fed ($n = 4$) or HFD-fed ($n = 6$), Flox or KO mice. Statistical analysis indicated no significant diet or genotype effects. *H*: NE and DA levels in eWAT extracts from NCD-fed ($n = 4$) or HFD-fed ($n = 6$), Flox or KO mice determined by UPLC normalized per milligram of protein. Significant diet and genotype effects ($P = 0.0122$ and $P = 0.0002$, respectively) for NE, and a significant genotype effect ($P = 0.0005$) for DA. *I*: Basal and stimulated serum glycerol levels (mmol/L) 15 min after CL-316,243 injection (1 mg/kg) normalized to adipose tissue weight. Significant diet and genotype effects ($P < 0.0001$ and $P = 0.0010$, respectively) for basal glycerol, and a significant diet effect ($P < 0.0001$) for stimulated levels. *J*: Relative (Rel) mRNA levels of β-3AR (*Adrb3)* in eWAT and iWAT of NCD- or HFD-fed Flox and KO mice by QPCR ($n = 5–8$ for eWAT groups, $n = 5–7$ for iWAT groups). Flox and KO mice fed an NCD are shown in green and red, respectively; Flox and KO mice fed an HFD are shown in cyan and orange, respectively. Significant group and tissue effects ($P < 0.0001$ and $P = 0.0240$, respectively). *K* and *L*: Expression of the catecholamine transporter genes *Slc22a3* (OCT3) and *Slc6a2* (NET), and catecholamine degradation enzymes monoamine-oxidase A (*Maoa)* and catecholamine-*O*-methyl transferase (*Comt)* in eWAT and iWAT of NCD-fed ($n = 5$) or HFD-fed ($n = 8$) Flox and KO mice by QPCR. We found significant genotype effect and diet-genotype interaction ($P = 0.0069$ and $P = 0.0019$, respectively) for *Slc22a3*, a significant genotype effect ($P = 0.0404$) for *Slc6a2*, significant diet and genotype effects ($P = 0.0012$ and $P = 0.0014$, respectively) for *Maoa*, and significant diet and genotype effects ($P = 0.0203$ and $P = 0.0006$, respectively) for *Comt*. Data are represented as mean ± SEM, asterisks indicate statistical significance by one-way or two-way ANOVA unless otherwise stated, with Tukey post hoc comparisons as appropriate. $*P < 0.05$, $**P < 0.01$, $***P < 0.001$, $****P < 0.0001$. Rel, relative.

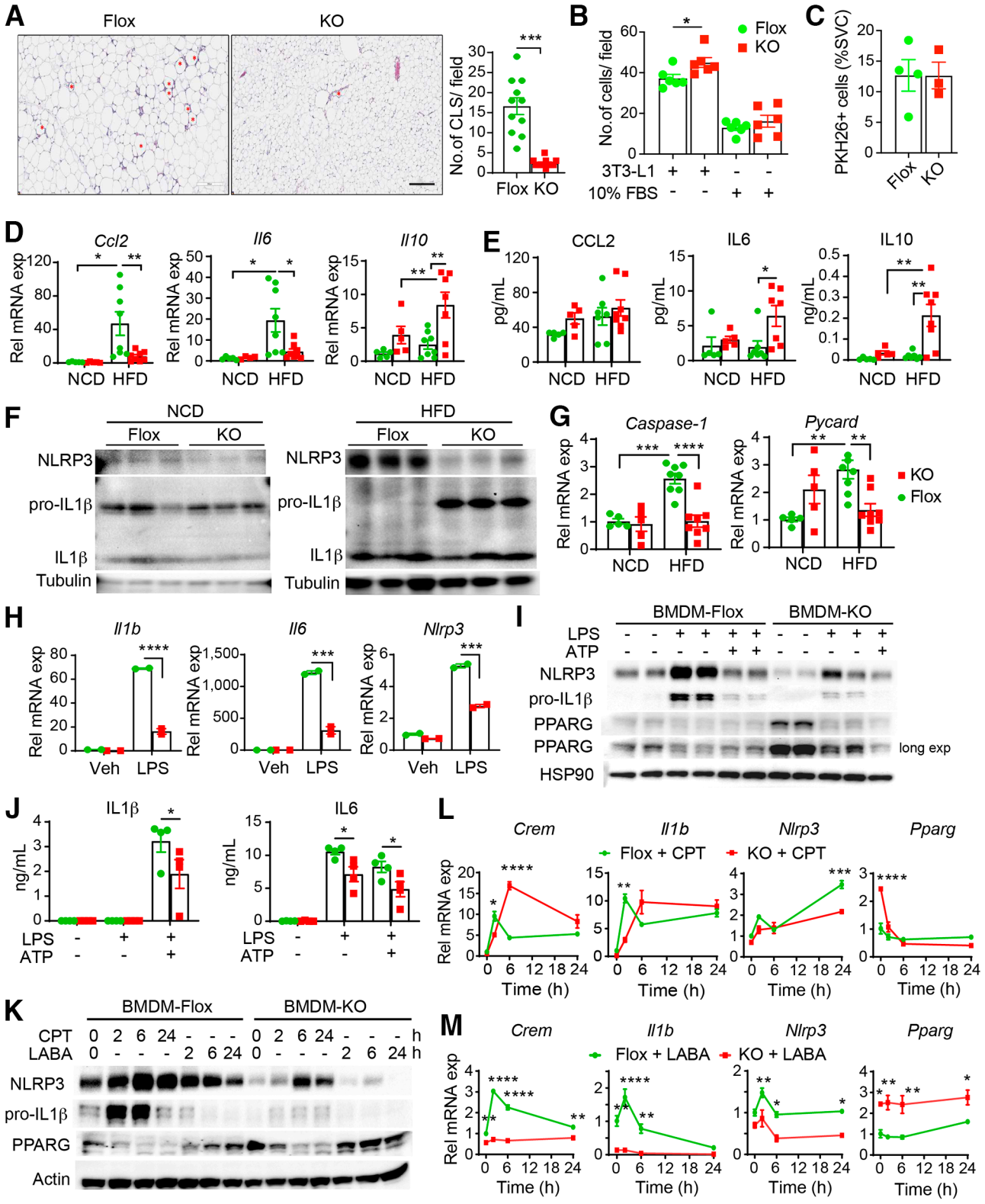

Figure 6—Reduced adipose tissue inflammation in *Gnas*$^{\Delta CD11c}$ KO mice. *A*: Representative hematoxylin and eosin (H&E) staining of sections of eWAT tissue. Crown-like structures (CLS) are indicated with red asterisks. Graph shows quantification of CLS density of the H&E–stained sections (n = 4/group). Flox mice are shown in green, KO mice in red. *B*: Migration of BMDMs from Flox or KO mice in Transwells in response to 3T3-L1 conditioned medium or serum. *C*: In vivo migration of PKH26-labeled BMDMs into WAT. *D*: Relative (Rel) mRNA expression (exp), by QPCR, of *Ccl2*, *Il6*, and *Il10* in eWAT from KO and Flox mice fed with NCD or HFD for 8 weeks (n = 5–8/group). Two-way ANOVA indicated a significant diet effect for *Il6* (P = 0.0135) and diet and genotype effects for *Il10* (P = 0.0368 and 0.0032, respectively) *E*: Plasma protein and tissue mRNA levels for CCL2, IL6, and IL10 in Flox and KO mice (n = 5–8/group). Two-way ANOVA indicated significant genotype effect for IL6 (P = 0.034), diet, genotype effects, and interaction for IL10 (P = 0.0128, 0.0052, and 0.0303,

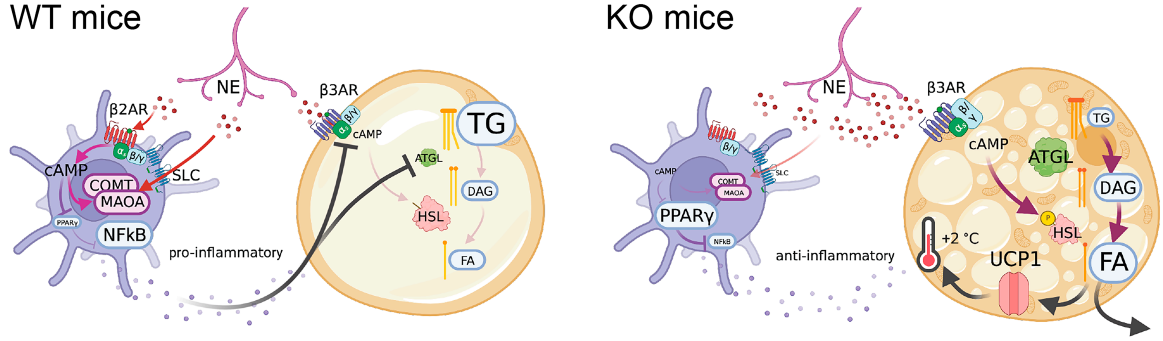

Figure 7—Model for immune cell–adipocyte crosstalk. Obesity increases NE signaling via β-2AR, Gαs, and cAMP in immune cells stimulating catecholamine transport and metabolism genes, repressing PPARγ and inducing inflammatory signaling and cytokine production. These inflammatory signals act on adjacent adipocytes to repress β-3AR and ATGL, thus reducing NE signaling and impairing lipolysis. Loss of Gαs in the immune cell prevents repression of PPARγ, reduces catecholamine transport and metabolism, and creates an anti-inflammatory environment that allows NE signaling via β-3AR, stimulation of lipolysis, and beiging of the adipocytes.

(8,26–28). Conversely, adipose tissue denervation eliminates the thermogenic response to a wide variety of stimuli, including fasting and cold exposure (6). Interestingly, complete loss of catecholamine production, however, has no effect on DIO and the mice have normal glucose tolerance (29) suggesting that the ratio of β- to α-adrenergic signaling is important. Many of the changes that we observe can be explained by elevated adrenergic signaling because β-3AR–specific agonists, which activate Gαs signaling in adipocytes, rescue metabolic dysfunction in mice (30–32), cause beiging of WAT (33), and enhance lipolysis and insulin secretion (34), and β-3AR KO mice are more susceptible to DIO (35,36). Similarly, β-2AR–specific antagonists that would inhibit Gαs signaling in immune cells improve glucose and insulin tolerance without affecting BW (37).

The human data are less clear but generally agree with the animal data (38,39). Humans have a different distribution of BAT than rodents (40), but BAT activation has been proposed as an antiobesity therapy (38,41). Catecholamine reuptake inhibitors cause weight loss by increasing thermogenesis (42), and high urinary catecholamine levels are inversely associated with obesity (43). Conversely, patients taking β-blockers have decreased energy expenditure and increased BW (44). In humans, the β3-agonist mirabegron improves glucose homeostasis, but side effects of β-agonist therapy include an increase in macrophage infiltration into adipose tissue and potential increases in blood pressure (45,46).

Last, the identity of the $CD11c^{+}$ innate immune cells that are responsible for our observed phenotype remains to be determined. Whether a recently identified population of sympathetic nerve–associated $CD11c^{+}$ macrophages (47) are responsible for our lean phenotype is unclear, because deletion of Gαs using LysM-Cre did not have the same phenotype. A limitation, however, is that LysM-Cre is not expressed in all macrophages (48). There is also a potential role for inflammation in the lean phenotype. The most striking change in cytokines in our KO mice was the strong elevation of IL-10 levels, which could potentially reverse obesity and improve glucose and insulin resistance (49,50). The role for IL-10 in obesity is controversial, however, because mice lacking IL-10 have increased thermogenesis (51,52). Results may be different in humans, however, because IL-10 has no effect on human adipocytes, although it has anti-inflammatory effects on immune cells (53).

Acknowledgments. We acknowledge the assistance of Dr. Valeria Estrada and the Biorepository and Tissue Technology Shared Resource at the Moores Cancer Center.

Funding. This work was funded primarily by National Institutes of Health (NIH) grants R01HL141999, U01AI125860, and R01CA196853 to E.R. and

respectively). *F*: Western blot for NLRP3, pro-IL-1β, and β-tubulin as a loading control in eWAT extracts from Flox and KO mice fed with NCD or HFD. *G*: Caspase-1 (*Casp1*) and ASC (*Pycard*) gene expression in eWAT from Flox and KO mice fed with NCD or HFD. Two-way ANOVA indicated significant diet and genotype effects and interaction for *Caspase1* ($P = 0.00027$, 0.0008, and $P = 0.0009$, respectively), and a significant diet–genotype interaction for *Pycard* ($P = 0.0008$). *H*: Relative mRNA expression, by QPCR, of *Il1b*, *Il6*, and *Nlrp3* in BMDMs from Flox and KO mice treated with vehicle (Veh) or LPS (100 ng/mL) for 18 h. *I*: BMDMs from Flox or KO mice treated with $LPS^{+/-}$ ATP (5 mmol/L; 1 h) immunoblotted for NLRP3, pro-IL1β, PPARG, and β-actin. A longer exposure of the PPARG blot is provided. *J*: IL1β and IL6 levels in the supernatants from BMDMs in (*I*) by ELISA. *K*: BMDMs from Flox or KO mice treated with a cell-permeable cAMP analog (CPT; 50 μmol/L) or the LABA formoterol (1 μmol/L) for increasing times immunoblotted for NLRP3, pro-IL1β, PPARG, and β-Actin. *L*: Time course of *Crem*, *Il1b*, *Nlrp3*, and *Pparg* gene expression in Flox or KO BMDMs treated with CPT. *M*: Time course of *Crem*, *Il1b*, *Nlrp3*, and *Pparg* gene expression in Flox or KO BMDMs treated with LABA. In all cases, Flox mice or cells are shown in green and KO mice or cells are in red. Data are presented as mean ± SEM, and asterisks indicate statistical significance by unpaired Student *t* test or two-way ANOVA as appropriate. $*P < 0.05$, $**P < 0.01$, $***P < 0.001$, $****P < 0.0001$. Rel, relative; Veh, vehicle.

N.J.G.W., and, in part, by a VA Merit Review Award I01BX004848 and Senior Research Career Scientist Award IBX005224 to N.J.G.W. The research was also supported by the NIH Cancer Center Support grant P30CA023100, the Diabetes Research Center grant P30DK063491, and the San Diego Digestive Disease Center grant P30DK120515. The ANCOVA analysis of calorimetric data done for this work was provided by the National Institute of Diabetes and Digestive and Kidney Diseases Mouse Metabolic Phenotyping Centers (www.mmpc.org) using their Energy Expenditure Analysis page (https://www.mmpc.org/shared/regression.aspx) and supported by grants DK076169 and DK115255.

Duality of Interest. No potential conflicts of interest relevant to this article were reported.

Author Contributions. E.R. and N.J.G.W. designed and conceived the study. L.Z. performed the experiments with the assistance of S.M.L. L.Z. was supported and mentored by A.T. D.S.H. assisted with animal husbandry. M.D. assisted with the glucose and insulin tolerance tests. S.B. assisted with cytokine measurements. L.E. performed the microbiota experiments. S.M. measured catecholamine levels and substrate uptake assays. M.H., J-W.B., and P.W. assisted with tissue harvest. A.J.A.M. performed the Seahorse measurements, S.D. and H.H.P. performed the Oroboros measurements. O.O. performed the cold-room thermogenesis assay. M.C. assisted with genotyping. L.Z. and N.J.G.W. wrote the manuscript and generated the figures. N.J.G.W. is the guarantor of this work and, as such, had full access to all the data in this study and takes responsibility for the integrity of the data and accuracy of the data analysis.

References

1. Xu H, Barnes GT, Yang Q, et al. Chronic inflammation in fat plays a crucial role in the development of obesity-related insulin resistance. J Clin Invest 2003;112:1821–1830

2. Ferrante AW Jr. The immune cells in adipose tissue. Diabetes Obes Metab 2013;15(Suppl. 3):34–38

3. Weisberg SP, McCann D, Desai M, Rosenbaum M, Leibel RL, Ferrante AW Jr. Obesity is associated with macrophage accumulation in adipose tissue. J Clin Invest 2003;112:1796–1808

4. Patsouris D, Li PP, Thapar D, Chapman J, Olefsky JM, Neels JG. Ablation of CD11c-positive cells normalizes insulin sensitivity in obese insulin resistant animals. Cell Metab 2008;8:301–309

5. Shi F, Collins S. Second messenger signaling mechanisms of the brown adipocyte thermogenic program: an integrative perspective. Horm Mol Biol Clin Investig 2017;31:20170062

6. Bartness TJ, Liu Y, Shrestha YB, Ryu V. Neural innervation of white adipose tissue and the control of lipolysis. Front Neuroendocrinol 2014;35:473–493

7. Bartness TJ, Shrestha YB, Vaughan CH, Schwartz GJ, Song CK. Sensory and sympathetic nervous system control of white adipose tissue lipolysis. Mol Cell Endocrinol 2010;318:34–43

8. Zeng W, Pirzgalska RM, Pereira MM, et al. Sympathetic neuro-adipose connections mediate leptin-driven lipolysis. Cell 2015;163:84–94

9. Bachman ES, Dhillon H, Zhang CY, et al. betaAR signaling required for diet-induced thermogenesis and obesity resistance. Science 2002;297:843–845

10. Cypess AM, Kahn CR. Brown fat as a therapy for obesity and diabetes. Curr Opin Endocrinol Diabetes Obes 2010;17:143–149

11. Harms M, Seale P. Brown and beige fat: development, function and therapeutic potential. Nat Med 2013;19:1252–1263

12. Lee J, Kim TH, Murray F, et al. Cyclic AMP concentrations in dendritic cells induce and regulate Th2 immunity and allergic asthma. Proc Natl Acad Sci USA 2015;112:1529–1534

13. Das M, Ellies LG, Kumar D, et al. Time-restricted feeding normalizes hyperinsulinemia to inhibit breast cancer in obese postmenopausal mouse models. Nat Commun 2021;12:565

14. Mina AI, LeClair RA, LeClair KB, Cohen DE, Lantier L, Banks AS. CalR: a web-based analysis tool for indirect calorimetry experiments. Cell Metab 2018;28:656–666.e1

15. Zimmermann R, Strauss JG, Haemmerle G, et al. Fat mobilization in adipose tissue is promoted by adipose triglyceride lipase. Science 2004;306:1383–1386

16. Yang CC, Wu CH, Lin TC, et al. Inhibitory effect of PPARγ on NLRP3 inflammasome activation. Theranostics 2021;11:2424–2441

17. Meng QQ, Feng ZC, Zhang XL, et al. PPAR-γ activation exerts an anti-inflammatory effect by suppressing the NLRP3 inflammasome in spinal cord-derived neurons. Mediators Inflamm 2019;2019:6386729

18. Wang L, Pydi SP, Cui Y, et al. Selective activation of G_s signaling in adipocytes causes striking metabolic improvements in mice. Mol Metab 2019;27:83–91

19. Leiss V, Schönsiegel A, Gnad T, et al. Lack of $G\alpha_{i2}$ proteins in adipocytes attenuates diet-induced obesity. Mol Metab 2020;40:101029

20. Li YQ, Shrestha YB, Chen M, Chanturiya T, Gavrilova O, Weinstein LS. Gsα deficiency in adipose tissue improves glucose metabolism and insulin sensitivity without an effect on body weight. Proc Natl Acad Sci USA 2016;113:446–451

21. Chen M, Chen H, Nguyen A, et al. G(s)alpha deficiency in adipose tissue leads to a lean phenotype with divergent effects on cold tolerance and diet-induced thermogenesis. Cell Metab 2010;11:320–330

22. Russo B, Menduni M, Borboni P, Picconi F, Frontoni S. Autonomic nervous system in obesity and insulin-resistance-the complex interplay between leptin and central nervous system. Int J Mol Sci 2021;22:5187

23. Esler M, Rumantir M, Wiesner G, Kaye D, Hastings J, Lambert G. Sympathetic nervous system and insulin resistance: from obesity to diabetes. Am J Hypertens 2001;14:304S–309S

24. Kim M, Bae S, Lim KM. Impact of high fat diet-induced obesity on the plasma levels of monoamine neurotransmitters in C57BL/6 mice. Biomol Ther (Seoul) 2013;21:476–480

25. Braun K, Oeckl J, Westermeier J, Li Y, Klingenspor M. Non-adrenergic control of lipolysis and thermogenesis in adipose tissues. J Exp Biol 2018;221(Suppl. 1):eb165381

26. Matthews VB, Rudnicka C, Schlaich MP. A cautionary note for researchers treating mice with the neurotransmitter norepinephrine. Biochem Biophys Rep 2018;15:103–106

27. Herat LY, Schlaich MP, Matthews VB. Sympathetic stimulation with norepinephrine may come at a cost. Neural Regen Res 2019;14:977–978

28. Mahú I, Barateiro A, Rial-Pensado E, et al. Brain-sparing sympathofacilitators mitigate obesity without adverse cardiovascular effects. Cell Metab 2020;31:1120–1135.e7

29. Ste Marie L, Luquet S, Curtis W, Palmiter RD. Norepinephrine- and epinephrine-deficient mice gain weight normally on a high-fat diet. Obes Res 2005;13:1518–1522

30. Borst SE, Hennessy M. Beta-3 adrenergic agonist restores skeletal muscle insulin responsiveness in Sprague-Dawley rats. Biochem Biophys Res Commun 2001;289:1188–1191

31. Clookey SL, Welly RJ, Shay D, et al. Beta 3 adrenergic receptor activation rescues metabolic dysfunction in female estrogen receptor alpha-null mice. Front Physiol 2019;10:9

32. Poher AL, Veyrat-Durebex C, Altirriba J, et al. Ectopic UCP1 overexpression in white adipose tissue improves insulin sensitivity in Lou/C Rats, a model of obesity resistance. Diabetes 2015;64:3700–3712

33. Fujimoto Y, Hashimoto O, Shindo D, et al. Metabolic changes in adipose tissues in response to β_3 -adrenergic receptor activation in mice. J Cell Biochem 2019;120:821–835

34. Heine M, Fischer AW, Schlein C, et al. Lipolysis triggers a systemic insulin response essential for efficient energy replenishment of activated brown adipose tissue in mice. Cell Metab 2018;28:644–655.e4

35. Preite NZ, Nascimento BP, Muller CR, et al. Disruption of beta3 adrenergic receptor increases susceptibility to DIO in mouse. J Endocrinol 2016;231:259–269

36. Valet P, Grujic D, Wade J, et al. Expression of human alpha 2-adrenergic receptors in adipose tissue of beta 3-adrenergic receptor-deficient mice promotes diet-induced obesity. J Biol Chem 2000;275:34797–34802
37. Nguyen LV, Ta QV, Dang TB, et al. Carvedilol improves glucose tolerance and insulin sensitivity in treatment of adrenergic overdrive in high fat diet-induced obesity in mice. PLoS One 2019;14:e0224674
38. Arch JR. Challenges in β(3)-adrenoceptor agonist drug development. Ther Adv Endocrinol Metab 2011;2:59–64
39. Cannavo A, Koch WJ. Targeting β3-adrenergic receptors in the heart: selective agonism and β-blockade. J Cardiovasc Pharmacol 2017;69: 71–78
40. Pan R, Zhu X, Maretich P, Chen Y. Metabolic improvement via enhancing thermogenic fat-mediated non-shivering thermogenesis: from rodents to humans. Front Endocrinol (Lausanne) 2020;11:633
41. Cypess AM, Weiner LS, Roberts-Toler C, et al. Activation of human brown adipose tissue by a β3-adrenergic receptor agonist. Cell Metab 2015;21: 33–38
42. Billes SK, Cowley MA. Catecholamine reuptake inhibition causes weight loss by increasing locomotor activity and thermogenesis. Neuropsychopharmacology 2008;33:1287–1297
43. An Y, Reimann M, Masjkur J, et al. Adrenomedullary function, obesity and permissive influences of catecholamines on body mass in patients with chromaffin cell tumours. Int J Obes 2019;43:263–275
44. Lee P, Kengne AP, Greenfield JR, Day RO, Chalmers J, Ho KK. Metabolic sequelae of β-blocker therapy: weighing in on the obesity epidemic? Int J Obes 2011;35:1395–1403
45. Finlin BS, Memetimin H, Zhu B, et al. The β3-adrenergic receptor agonist mirabegron improves glucose homeostasis in obese humans. J Clin Invest 2020;130:2319–2331
46. O'Mara AE, Johnson JW, Linderman JD, et al. Chronic mirabegron treatment increases human brown fat, HDL cholesterol, and insulin sensitivity. J Clin Invest 2020;130:2209–2219
47. Pirzgalska RM, Seixas E, Seidman JS, et al. Sympathetic neuron-associated macrophages contribute to obesity by importing and metabolizing norepinephrine. Nat Med 2017;23:1309–1318
48. Shi J, Hua L, Harmer D, Li P, Ren G. Cre driver mice targeting macrophages. Methods Mol Biol 2018;1784:263–275
49. Nakata M, Yamamoto S, Okada T, et al. IL-10 gene transfer upregulates arcuate POMC and ameliorates hyperphagia, obesity and diabetes by substituting for leptin. Int J Obes 2016;40:425–433
50. Hong EG, Ko HJ, Cho YR, et al. Interleukin-10 prevents diet-induced insulin resistance by attenuating macrophage and cytokine response in skeletal muscle. Diabetes 2009;58:2525–2535
51. Rajbhandari P, Arneson D, Hart SK, et al. Single cell analysis reveals immune cell-adipocyte crosstalk regulating the transcription of thermogenic adipocytes. eLife 2019;8:e49501
52. Rajbhandari P, Thomas BJ, Feng AC, et al. IL-10 signaling remodels adipose chromatin architecture to limit thermogenesis and energy expenditure. Cell 2018;172:218–233.e17
53. Acosta JR, Tavira B, Douagi I, et al. Human-specific function of IL-10 in adipose tissue linked to insulin resistance. J Clin Endocrinol Metab 2019;104: 4552–4562